Electrical Evolution of p-Type SnO_x Film and Transistor Deposited by RF Magnetron Sputtering

Yuyan Zhou, Yu Song, Ruohao Hong, Xingqiang Liu, Xuming Zou, Benjamin Iñíguez, *Fellow, IEEE*, Denis Flandre, *Senior Member, IEEE*, Guoli Li, and Lei Liao, *Senior Member, IEEE*

***Abstract*— In this work, by altering oxygen partial pressure (OPP) and sputtering power (P_{RF}) of the radio frequency (RF) magnetron sputtering process, we investigate electrical evolution of the p-type SnO_x film and transistor. Herein, combining device current–voltage (such as ON-state current and field-effect mobility), low-frequency noise (LFN), and gate-bias-stress characteristics, we find that the optimal OPP range is 4.8%–7.2% for the SnO_x film deposition at P_{RF} of 70 and 30 W. Based on X-ray photoelectron spectroscopy (XPS), the SnO_x films deposited at high power (70 W) show less sensitivity to OPP, which leads to the slow transition of internal Sn^{2+}, Sn^{4+} states, and a relatively large process window. Furthermore, the defect states inside the SnO_x are analyzed. The oxygen interstitials (O_i), as deep acceptors, keep inactive regardless of the external bias. The oxygen vacancies (Vo) and the ionized Vo^{2+} states, which act as the electron traps, get suppressed and are attributed to the ambipolar behavior in the SnO_x transistor, while increasing the OPP. This work benefit lies in a comprehensive analysis of the sputtering process parameters impact on SnO_x film and transistor properties and their underlying defects.**

***Index Terms*— Defects, electrical characteristics, metal-oxide semicondutors (MOs), sputtering, thin-film transistors (TFTs).**

I. Introduction

METAL–OXIDE–SEMICONDUCTORS (MOs) have made an impressive progress in the recent decades and been used as semiconducting channel of thin-film transistors (TFTs) in the display applications [1], [2], because of their relatively high carrier mobility, low deposition temperature and cost, large-area uniformity, excellent process compatibility, and so on [1]. However, unlike industrialization of the n-type (e.g., InGaZnO) TFTs [3], [4], the development of the high-performance p-type MOs film and device still lags a lot [5], which hinders the CMOS circuit design and fabrication. In the p-type MOs, the transport path for holes is mainly attributed to the anisotropic and localized O 2p orbitals at valence band maximum (VBM), leading to a large hole effective mass and low carrier mobility [1], [5]. As it is reported, the promising p-type oxides that have been extensively studied are tin monoxide (SnO), copper oxide (Cu_2O or CuO), and nickel oxide (NiO) [6], [7], [8], [9]. Among them, there is a relatively higher hole mobility in SnO due to the creation of a suitable dispersed VBM by hybridization of the Sn 5s and O 2p orbitals [1], [5], [10]. Nevertheless, SnO also holds some disadvantages, for example, the Sn^{2+} states are thermodynamically metastable [11], and may be reduced to the metallic Sn (Sn^0) or oxidized to the Sn^{4+} states. That means, the Sn^0, Sn^{2+}, and Sn^{4+} states co-exist in the SnO film, leading to the SnO_x phases. According to the experimental observations, the optimal property of the thin film often occurs when SnO_x occurs as mixed phases of Sn, SnO, and SnO_2 [12]. Therefore, considerable efforts have been made to study the growth conditions to optimize the SnO_x film quality as well as the TFT performance [1], [11], [13], [14]. The impact of oxygen partial pressure (OPP) on the formation of oxide phase (SnO, mixed-phase SnO, or SnO_2) and the amount of metallic Sn have been investigated in [13], in which a well-controlled amount of metallic tin (deposited at 1.8 mtorr and with OPP = 9%) can substantially increase the hole mobility. While altering the OPP, the phase change pattern and the n- or p-type conductivity of the SnO_x films are also investigated in [11] and [14], but the device performances are still largely behind. In [15], a sensitive dependence of electronic property and stoichiometry of the SnO_x film on sputtering deposition power have been experimentally investigated. However, in these researches, there is no complete analysis of defect states inside the SnO_x [11], [16], with respect to the deposition parameters and the film or device electrical properties. Therefore, in this study, we alter the OPP and reactive sputtering power to

Manuscript received 14 March 2023; accepted 4 April 2023. Date of publication 21 April 2023; date of current version 25 May 2023. This work was supported in part by the National Natural Science Foundation of China under Grant 62004065, in part by the National Key Research and Development Program of Ministry of Science and Technology (MOST) under Grant 2022YFE041500, and in part by Wallonie-Bruxelles/China (MOST) Cooperation Project. The review of this article was arranged by Editor Y. Uraoka. *(Corresponding author: Guoli Li.)*

Yuyan Zhou, Yu Song, Ruohao Hong, Xuming Zou, and Guoli Li are with The School of Physics and Electronics, Hunan University, Changsha 410082, China (e-mail: liguoli_lily@hnu.edu.cn).

Xingqiang Liu and Lei Liao are with the College of Semiconductors (College of Integrated Circuits), Hunan University, Changsha 410082, China.

Benjamin Iñíguez is with the Departament d'Enginyeria Electrònica, Elèctrica i Automàtica, Universitat Rovira i Virgili, 43007 Tarragona, Spain.

Denis Flandre is with the Institute of Information and Communication Technologies, Electronics and Applied Mathematics (ICTEAM), Université Catholique de Louvain, 1348 Leuven-la-Neuve, Belgium.

Color versions of one or more figures in this article are available at https://doi.org/10.1109/TED.2023.3266417.

Digital Object Identifier 10.1109/TED.2023.3266417

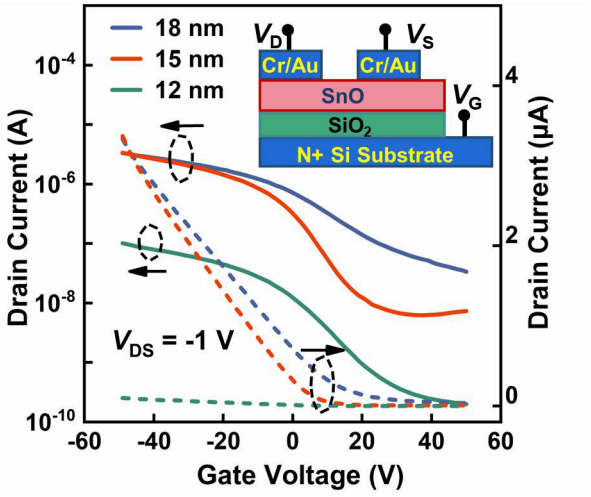

Fig. 1. Transfer curves (I_{DS}–V_{GS}, at $V_{DS} = -1.0$ V) of the SnO_x TFTs with different channel thicknesses fabricated at OPP = 3.6% and P_{RF} = 70 W. Device structure of the as-fabricated TFT shown in inset.

deposit the SnO_x films and transistors. Combining with the electrical characterizations (e.g., transfer and output curves of TFTs), X-ray photoelectron spectroscopy (XPS), grazing incident X-ray diffraction (GIXRD), and low-frequency noise (LFN) measurements, we figure out the impact of sputtering parameter and obtain a clear and comprehensive map of the intrinsic defects distribution inside SnO_x.

II. Experimental Fabrication and Characterization

The SnO_x TFT fabricated in this work has a bottom-gate staggered structure, as shown in Fig. 1. A heavily doped n-type silicon wafer with a thermally grown 100-nm-thick SiO_2 was used as the bottom gate and the corresponding gate dielectric layer. The SnO_x channel layer was deposited by reactive radio frequency (RF) magnetron sputtering, using a 99.99% metal Sn target. To investigate the variation in SnO_x film quality as well as the device characteristics, the OPP ratio (which was defined as the relative oxygen flow rate of $[O_2]/([Ar] + [O_2])$, with a fixed O_2 ratio of 30% in the $([Ar] + [O_2])$ gas flow) was varied from 2.4% to 9.6%, and the sputtering powers P_{RF} of 30 and 70 W were chosen as the representative cases, as no sensitive dependence of the p-type film quality on P_{RF} was observed in our experiments. The deposition pressure was fixed at 6 mtorr. The SnO_x films were deposited at room temperature (RT) and then annealed at 250 °C for 10 min to achieve the optimal microstructure and quality [17]. Finally, a 50-nm Au/10-nm Cr film was deposited by thermal evaporation (using metal shadow masks) as the source and drain electrodes. Channel width (W) and length (L) of the SnO_x TFTs were 140 and 140 μm, respectively. The electrical characteristics of the SnO_x TFTs were measured by using a semiconductor characterization system (Keithley 4200) at RT. All the electrical parameters, e.g., threshold voltage V_{TH}, field-effect mobility μ_{EF}, and subthreshold slope (SS), were extracted at forward sweep from OFF-state to ON-state of the TFTs.

TABLE I
Electrical Parameters of the SnO_x TFTs Deposited at 70 W

SnOx thickness d (nm)	I_{ON} (A)	μ_{LIN} (cm²/Vs)	I_{OFF} (A)	SS (V/dec)
12	1.07E-7	0.05	1.78E-10	13.13
15	3.37E-6	1.7	6.26E-9	11.0
18	3.34E-6	1.7	3.37E-8	26.3

III. Results and Discussion

Fig. 1 shows the transfer curves (I_{DS}–V_{GS}, in logarithmic and linear scale) of the p-type SnO_x TFTs measured at drain bias $V_{DS} = -1.0$ V, in which the different channel thicknesses d = 12, 15, and 18 nm were obtained via controlling the sputtering time (45, 50, and 55 s, separately) at the fixed P_{RF} of 70 W. Here, the thin-film thickness d was measured by atomic force microscope (AFM) technique. Correspondingly, key parameters (e.g., ON-state current I_{ON}, linear mobility μ_{LIN}, OFF-state current I_{OFF}, and SS) of the SnO_x TFTs are extracted in Table I. The TFT ON-state current (I_{ON}) can achieve a reasonably high value of $>10^{-6}$ A, in the cases of d = 15 and 18 nm, but sharply decreased at d = 12 nm, which can be attributed to the degraded quality (microstructure disorder) of the SnO_x film. The linear mobility μ_{LIN} maintains a stable value of 1.7 cm²/Vs (d = 15 and 18 nm) and then falls down to an extremely low value at d = 12 nm. The OFF-state current (I_{OFF}) also shows its strong dependence on d and is reduced from 3.37×10^{-8} to 1.78×10^{-10} A, while decreasing d from 18 to 12 nm. Based on the channel depletion mechanism [18], in the OFF-state, holes in p-type SnO_x film are depleted by the applied positive gate bias (V_{GS}). Therefore, thinner film with lower holes density is the main reason for the decrease of OFF-state current in Fig. 1. As well, an enhanced gate control is also observed with the decreased d, in which SS is improved from 26.3 to 11.0 V/dec. Therefore, the estimated width of the depletion layer for our SnO_x TFTs is ~15 nm in this work, which corresponds to a maximum channel thickness that can control the carrier depletion and the density.

Fig. 2(a) and (b) and (d) and (e) shows the transfer curves (I_{DS}–V_{GS}, at drain bias $V_{DS} = -1.0$ V) of the 15-nm-thick SnO_x TFTs fabricated at RF sputtering power (P_{RF}) of 70 and 30 W, respectively, in which the OPP is altered from 2.4% to 9.6%. Here, the SnO_x TFTs deposited at the high (P_{RF} = 70 W) and low (P_{RF} = 30 W) power present similar trends of electrical performance, when the OPP is varied. The ON-state current I_{ON} is improved as OPP increases and then gets degraded while OPP increasing up to the maximum value of 9.6%. Correspondingly, the OFF-state current I_{OFF} presents the similar "up-to-down" trend with the varied OPP. Moreover, the ambipolar behavior is observed in these p-type SnO_x TFTs. At high RF power of 70 W, the ambipolar behavior appears while increasing OPP $\geq$ 4.8%, whereas it also occurs in the low RF power (30 W) deposited SnO_x TFTs with OPP $>$ 7.2%. Fig. 2(c) and (f) plots the output curves (I_{DS}–V_{DS}, with the gate bias V_{GS} ranging from 50 to −50 V) of the SnO_x TFTs deposited at OPP = 4.8% and 7.2% (the optimal range of OPP which will be discussed next).

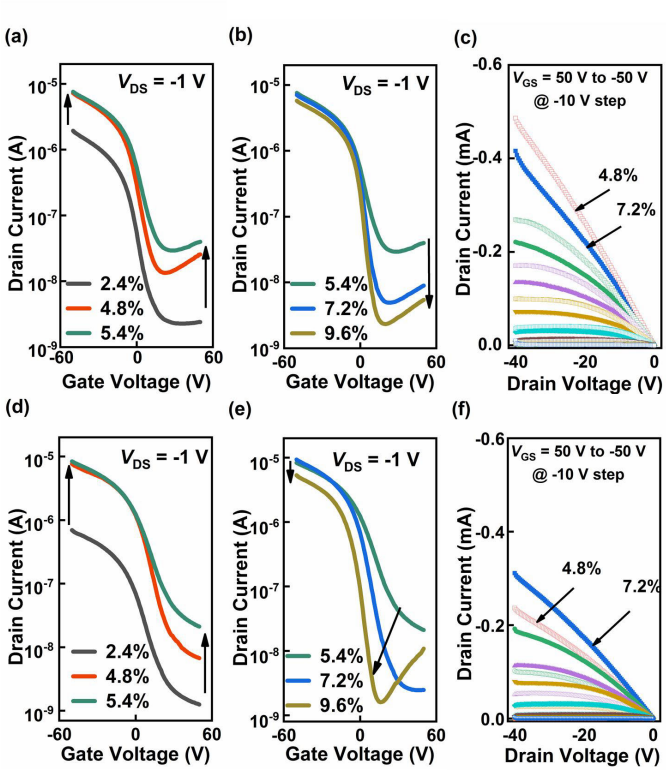

Fig. 2. Transfer curves (I_{DS}–V_{GS}, at $V_{DS} = -1.0$ V) of the 15-nm-thick SnO_x TFTs deposited at RF sputtering power (P_{RF}) of (a) and (b) 70 W and (d) and (e) 30 W, with the varied OPP of = 2.4%, 4.8%, 5.4%, 7.2%, and 9.6%. Output curves (I_{DS}–V_{DS}, with V_{GS} ranging from 50 to −50 V) of the SnO_x TFTs fabricated at (c) $P_{RF} = 70$ W and (f) $P_{RF} = 30$ W, with the representative OPP = 4.8% (unfilled dot) and 7.2% (filled dot).

Detailed device parameters are illustrated and summarized in Fig. 3 to investigate the influence of the RF power P_{RF} (70 and 30 W) and oxygen flow OPP (ranging from 2.4% to 9.6%) on the SnO_x TFTs. At 70 W [see Fig. 3(a)–(c)], the ON-state current I_{ON} is improved as OPP increases, then keep approximately stable (7.1–7.8 μA) within the OPP range of 4.8%–7.2%, and finally gets degraded. In the meantime, I_{OFF} presents the maximum value of 21 nA at OPP = 5.4% in Fig. 3(a). In comparison, a higher I_{ON} (8.0–9.4 μA) is presented in the 30-W-deposited SnO_x TFTs [see Fig. 3(d)], at OPP = 4.8%–7.2%. Therefore, considering industrial demand (high drive current, large ON/OFF ratio, and low operation voltage) for the display technology, we then focus on the OPP optimal range of 4.8%–7.2%. Within the optimal range (OPP = 4.8%–7.2%), the linear mobility μ_{LIN} is extracted to be 3.6–4.0 cm^2/Vs for $P_{RF} = 70$ W and 3.9–4.9 cm^2/Vs for $P_{RF} = 30$ W, showing an improvement by a factor of ∼2, compared to μ_{LIN} in Table I, where device is deposited at OPP = 3.6% and $P_{RF} = 70$ W, and these μ_{LIN} values are relatively competitive, compared with other studies [14], [16], [19]. SS shows the similar trend with I_{OFF}, in which the degraded, highest value is extracted at OPP = 5.4%, and then, SS gets optimized as OPP increases over 5.4%.

Fig. 3(b) and (e) shows the OPP impact on bias-stress-induced electrical instabilities of the SnO_x TFTs fabricated at $P_{RF} = 70$ and 30 W, respectively, under a gate bias stress of $V_{GS} = -15$ V and with stress durations of 100, 500, and 1000 s. Generally, the relatively stable negative-bias-stress (NBS) characteristics (i.e., the shift of threshold voltage ΔV_{TH} and SS) are observed. In the optimal range of OPP (4.8%–7.2%), NBS characteristics of the SnO_x TFT deposited at 70 W are slightly degraded with ΔV_{TH} changing from −2.1 to −2.5 V at the stress duration of 1000 s.

At low P_{RF} (30 W), NBS is optimized from $\Delta V_{TH} = -2.1$ to −1.0 V. In the meantime, the SS of the SnO_x TFTs deposited at $P_{RF} = 70$ W keeps around 12.0 V/dec for OPP = 4.8% and 11.0 V/dec for OPP = 7.2%, and the SS values of the TFTs deposited at $P_{RF} = 30$ W are 12.5 V/dec for OPP = 4.8% and 9.5 V/dec for OPP = 7.2%. Physically, there are two models to explain the V_{TH} shift (ΔV_{TH}): charge trapping or defect generation [20], [21]. Since the SS) did not change significantly during the NBS in this work, ΔV_{TH} can be attributed to charge trapping at the SnO_x channel/dielectric interface or within the gate dielectric layer [22], [23].

Correspondingly, the LFN characterizations in Fig. 3(c) and (f) can validate the performance improvement to the SnO_x TFTs, while altering the OPP at $P_{RF} = 70$ and 30 W. The lowest value of the LFN spectra density is obtained at OPP = 4.8% and 7.2%, compared to the cases of OPP = 2.4% and 9.6%. Meanwhile, the insets show the normalized S_{ID}/I_D^2 versus $|V_{GS} - V_{TH}|$ at a frequency of 20 Hz. A slope value of ∼2 indicates that the main mechanism of LFN is carrier number fluctuation model [24], which is related to the interface trap density (N_{it}). N_{it} can be extracted by $N_{it} = (S_{ID}C_{OX}^2 WLf(V_{GS} - V_{TH})^2\gamma/q^2kTI_{DS}^2)$ [25], where Cox is the capacitance per unit area, γ is the attenuation coefficient with a value of 10^8 cm^{-1}, q is the elementary electric charge, k is the Boltzmann constant, and T is the temperature [26]. The lowest value of N_{it} is approximately calculated to be 5–10 × 10^{22} eV^{-1}·cm^{-3} at high power ($P_{RF} = 70$ W) and to be 1–6 × 10^{22} eV^{-1}·cm^{-3} at $P_{RF} =$ 30 W. These values are all extracted in the OPP range of 4.8%–7.2%.

XPS and GIXRD measurements have been performed to analyze the chemical composition of the SnO_x films, deposited at $P_{RF} = 70$ and 30 W and with OPP ranging from 2.4% to 9.6%. According to the typical core-level spectra of Sn 3d and O 1s, the Sn $3d_{5/2}$ spectrum consists of the Sn^0 peak located at ∼484.4 eV, the Sn^{2+} peak at ∼485.9 eV, and the Sn^{4+} peak at ∼486.6 eV [27], the O 1s spectrum consists of the O_{Latt} peak located at ∼530.4 eV, the O_{Vac} peak at ∼531.8 eV, and the O_{Chem} peak at ∼532.8 eV [28]. In Fig. 4(a) and (d), we find out that the area percentage of Sn^{4+} becomes higher with the increased OPP, whereas the percentages of Sn^{2+} and Sn^0 get decreased, i.e., the Sn^{2+} state continues to be oxidized into the Sn^{4+} state. Here, while increasing OPP from 2.4% to 9.6%, the proportion of Sn^{2+} in the SnO_x film, which was deposited at $P_{RF} = 30$ W, gets decreased by 14.0% (i.e., decreased from 37.5% to 23.5%), and the proportion of Sn^{4+} increased by 16.3% (i.e., rising from 59.5% to 75.8%), respectively, compared to 4.4% and 5.3% at $P_{RF} = 70$ W. For such case, we can reasonably infer that the reactive sputtering power affects the process of phase transition between SnO (Sn^{2+}) and SnO_2 (Sn^{4+}), $2SnO + O_2 \rightarrow 2SnO_2$ [29]. In the meantime, the transition is accompanied by the oxidation of

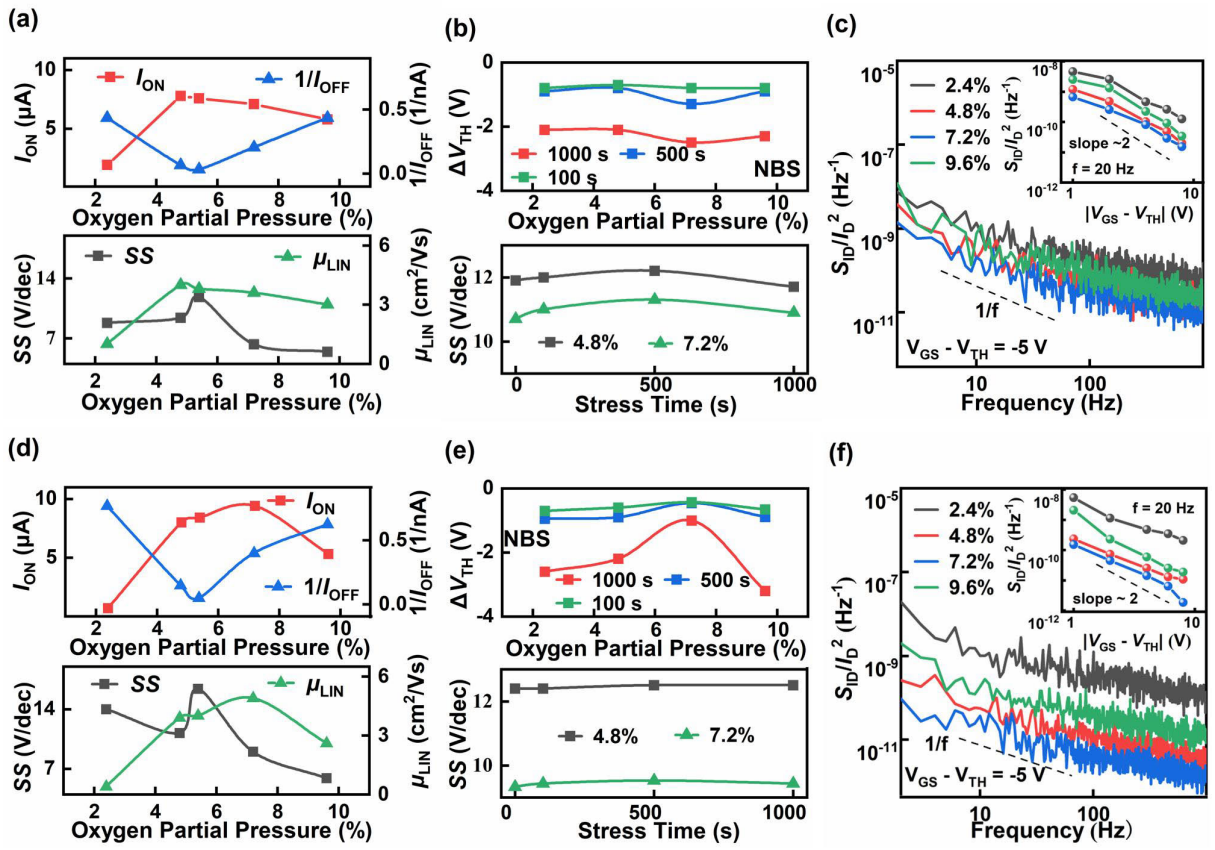

Fig. 3. (a) and (d) ON-state current I_{ON} and OFF-state current I_{OFF}, linear mobility μ_{LIN}, and SS, (b) and (e) threshold voltage shift ΔV_{TH} under NBS and SS, versus stress time, and (c) and (f) normalized LFN characteristics at $V_{GS}-V_{TH} = -5$ V and normalized S_{ID}/I_D^2 versus $|V_{GS} - V_{TH}|$ at 20 Hz of the SnO_x TFTs deposited at 70 and 30 W, respectively.

metallic Sn (Sn^0), Sn + $O_2 \rightarrow SnO_2$. At high-power P_{RF} (70 W), SnO_x seems to be less sensitive to oxygen, the internal chemical state transition is slower, and the chemical composition itself tends to be more stable. Correspondingly, the evolution of O 1s spectra is well consistent with that trend of Sn $3d_{5/2}$ spectra, as shown in Fig. 4(b) and (e). As OPP increases from 2.4% to 9.6%, the content of the O_{Latt} peak (consisting of the O–Sn^{2+} and O–Sn^{4+} components) at 70 W changes from 58.5% to 67.1%, whereas the oxygen vacancy (O_{Vac}) content decreases from 35.7% down to a minimum value of 24.2%. Similar trends are also observed in the case of 30 W, in which O_{Latt} increases from 53.8% to 64.1% and O_{Vac} decreases from 39.2% to 28.2%. The GIXRD patterns in Fig. 4(c) and (f) show the phase change in the SnO_x films deposited at $P_{RF} = 70$ and 30 W, respectively. The peaks of the β-Sn phase [14] are slightly detected at OPP = 2.4% and then get disappeared while increasing OPP. It is consistent with our XPS characterizations [see Fig. 4(a) and (d)], the Sn^0 components get decreased or oxidized while OPP increasing from 2.4% to 9.6%. The (101), (110), and (112) diffraction peaks of the α-SnO phase [30] are observed within 2.4%–7.2% of the OPP, indicating the polycrystalline formation. While OPP $\geq$ 9.6%, there are no characteristic peaks for any phases perceived, suggesting the amorphous nature of the films. The scanning electron microscopy (SEM) characterizations validate that the polycrystalline SnO_x films are converted into the amorphous ones while increasing OPP from 2.4% to 9.6% in our experiments.

To physically understand the device performance, the defect states inside the SnO_x film are schematically illustrated in Fig. 5, in which the bulk defects are represented by the sum of the tail and Gaussian states [31], [32]. Normally, the tail states are mainly composed of the donor-like defect states (N_{TD}) and acceptor-like defect states (N_{TA}). In the Gaussian distributed defects, Sn vacancies (V_{Sn}) act as shallow acceptors, lying at 0.12–0.13 eV above the VBM, which were often expected to contribute to the p-type conductivity inside the tin monoxide but turned out unlikely to form because of their high formation energy [33]. With energy level at ~0.07–0.1 eV above the VBM and much lower formation energy compared to that of the isolated V_{Sn}, the shallow-acceptor complexes (V_{Sn}–H) with the Sn vacancies and the unintentional impurities (i.e., hydrogen) offer an explanation for the observed p-type conductivity, as concluded in [33]. Regarding the oxygen-related defects, oxygen vacancies (V_O) are deep donors with a transition level occurring at 0.24 eV above the VBM and get ionized to form the Vo^{2+} charge state in p-type SnO_x. When the Fermi level (E_F) shifts away from VBM under a positive gate bias V_{GS}, the ionized Vo^{2+} will act as an electron trap (acceptor) and get negatively charged to form Vo^0. That means, the presence of tremendous oxygen-related (e.g., O_{Vac}) defects or subgap states would impede the E_F shifting from the energy level of near VBM to the vicinity of conduction-band minimum (CBM) because of the trapping and detrapping effect [34], [35]. Consequently, it leads to the absence of the ambipolar operation in the p-type SnO_x TFTs

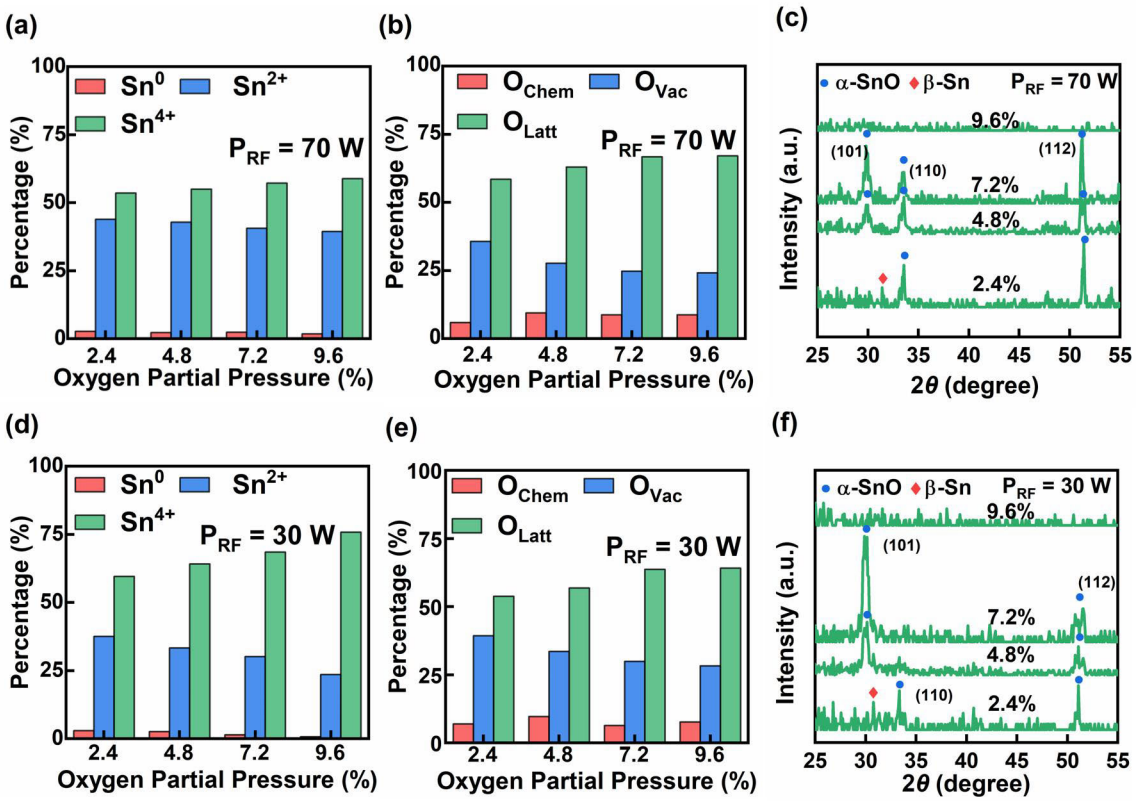

Fig. 4. (a) and (d) Area percentages of the Sn^0, Sn^{2+}, and Sn^{4+} components by deconvoluting the XPS Sn $3d_{5/2}$ profile, (b) and (e) area percentages of the O_{Latt}, O_{Vac}, and O_{Chem} peaks by deconvoluting the XPS O 1s profile, and (c) and (f) GIXRD spectra of the SnO_x TFTs deposited at 70 and 30 W.

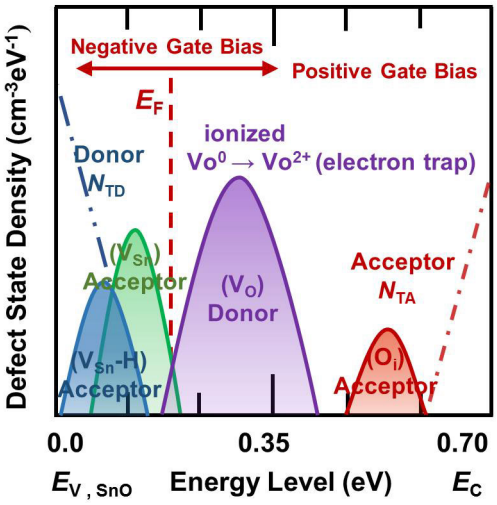

Fig. 5. Schematic illustration of defect states distribution in the p-type SnO_x film.

when a large $|V_{GS}|$ is applied. These are consistent with our experimental observations in Figs. 2 and 4, and the ambipolar behavior appears in the SnO_x TFTs while increasing OPP up to 4.8% (at RF power of 70 W) or 9.6% (at RF power of 30 W), with the reduced content of the O_{Vac} component in XPS (i.e., the oxygen vacancy defect V_O). Therefore, on the contrary to other discussion [36], we confirm that by reducing the oxygen vacancy and near-VBM defects, it is allowed to change the electrical characteristics from p-channel only conduction to ambipolar behavior. In the meantime, oxygen interstitials (O_i) keep electrically inactive and present in the neutral charge state for all the values of Fermi level E_F [37], while the back-gate bias (V_{GS}) is swept from the negative to the positive. Therefore, we conclude that O_i is one acceptor-like, deep defect in the p-type SnO_x.

IV. Conclusion

To summarize, we systematically investigated the impact of OPP and sputtering power (P_{RF}) on the electrical property of the SnO_x films and TFTs. ON-state currents I_{ON} of the SnO_x transistors deposited at P_{RF} = 70 and 30 W show a similar "up-to-down" trend, while OPP is varying from 2.4% to 9.6%. Within the optimal range of OPP of 4.8%–7.2%, the device field-effect mobility μ_{LIN} can be improved by a factor of ~2, compared to the transistors fabricated at the initial OPP of 3.6%. LFN characterizations confirm that the minimized noise spectra density and defect density N_{it} are achieved in the optimal OPP range. Based on the XPS measurements, it seems that the chemical states (e.g., the Sn^{2+} and Sn^{4+} components) of the SnO_x film sputtered at high-power P_{RF} of 70 W are less sensitive to oxygen, i.e., less oxidation or phase transition ($2SnO + O_2 \rightarrow 2SnO_2$), compared with the low-power (P_{RF} = 30 W) deposition. The GIXRD and SEM characterizations prove that the polycrystalline SnO_x films are converted into the amorphous nature while increasing OPP from 2.4% to 9.6% in the experiments. A complete description of defect states is finally presented for the SnO_x material system. We find that the oxygen interstitials (O_i) act as deep acceptors but turn to be inactive regardless of the external back-gate bias (V_{GS}).

The oxygen vacancies (V_O), as the deep donors which can get ionized to form the acceptor-like Vo^{2+} charge states, are effectively suppressed while increasing the OPP, resulting in the ambipolar behavior in the SnO_x TFTs. This work offers a physical interpretation of the electrical evolution of the SnO_x film and transistor to boost their further exploration and high-performance development.

REFERENCES

[1] Z. Wang, P. K. Nayak, J. A. C.-Frescas, and H. N. Alshareef, "Recent developments in p-type oxide semiconductor materials and devices," *Adv. Mater.*, vol. 28, no. 20, pp. 3831–3892, May 2016, doi: 10.1002/adma.201503080.

[2] K. Nomura, H. Ohta, A. Takagi, T. Kamiya, M. Hirano, and H. Hosono, "Room-temperature fabrication of transparent flexible thin-film transistors using amorphous oxide semiconductors," *Nature*, vol. 432, no. 4016, pp. 488–492, Nov. 2004, doi: 10.1038/nature03090.

[3] T. Kamiya, K. Nomura, and H. Hosono, "Present status of amorphous In–Ga–Zn–O thin-film transistors," *Sci. Technol. Adv. Mater.*, vol. 11, no. 4, Feb. 2010, Art. no. 044305, doi: 10.1088/1468-6996/11/4/044305.

[4] H. Chen, Y. Cao, J. Zhang, and C. Zhou, "Large-scale complementary macroelectronics using hybrid integration of carbon nanotubes and IGZO thin-film transistors," *Nature Commun.*, vol. 5, no. 1, pp. 1–12, Jun. 2014, doi: 10.1038/ncomms5097.

[5] E. Fortunato, P. Barquinha, and R. Martins, "Oxide semiconductor thin-film transistors: A review of recent advances," *Adv. Mater.*, vol. 24, no. 22, pp. 2945–2986, Jun. 2012, doi: 10.1002/adma.201103228.

[6] X. Zeng, M. Zhukova, S. Faniel, G. Li, and D. Flandre, "Room-temperature DC-sputtered p-type CuO accumulation-mode thin-film transistors gated by HfO_2," *Appl. Phys. Lett.*, vol. 121, no. 13, Sep. 2022, Art. no. 133503, doi: 10.1063/5.0098757.

[7] P. Wang, Y. H. Ng, and R. Amal, "Embedment of anodized p-type Cu_2O thin films with CuO nanowires for improvement in photoelectrochemical stability," *Nanoscale*, vol. 5, no. 7, pp. 2952–2958, Mar. 2013, doi: 10.1039/c3nr34012k.

[8] A. Liu et al., "Solution combustion synthesis: Low-temperature processing for p-type Cu: NiO thin films for transparent electronics," *Adv. Mater.*, vol. 29, no. 34, Jul. 2017, Art. no. 1701599, doi: 10.1002/adma.201701599.

[9] P. Gupta, T. Dutta, S. Mal, and J. Narayan, "Controlledp-type ton-type conductivity transformation in NiO thin films by ultraviolet-laser irradiation," *J. Appl. Phys.*, vol. 111, no. 1, Jan. 2012, Art. no. 013706, doi: 10.1063/1.3671412.

[10] Y. Ogo et al., "Tin monoxide as an S-orbital-based p-type oxide semiconductor: Electronic structures and TFT application," *Phys. Status Solidi A, Appl. Mater. Sci.*, vol. 206, no. 9, pp. 2187–2191, Jul. 2009, doi: 10.1002/pssa.200881792.

[11] H. Luo, L. Y. Liang, H. T. Cao, Z. M. Liu, and F. Zhuge, "Structural, chemical, optical, and electrical evolution of SnO_x films deposited by reactive Rf magnetron sputtering," *ACS Appl. Mater. Interfaces*, vol. 4, no. 10, pp. 5673–5677, Oct. 2012, doi: 10.1021/am301601s.

[12] C. Guillén and J. Herrero, "P-type SnO thin films prepared by reactive sputtering at high deposition rates," *J. Mater. Sci. Technol.*, vol. 35, no. 8, pp. 1706–1711, Aug. 2019, doi: 10.1016/j.jmst.2019.03.034.

[13] J. A. Caraveo-Frescas, P. K. Nayak, H. A. Al-Jawhari, D. B. Granato, U. Schwingenschlögl, and H. N. Alshareef, "Record mobility in transparent p-type tin monoxide films and devices by phase engineering," *ACS Nano*, vol. 7, no. 6, pp. 5160–5167, May 2013, doi: 10.1021/nn400852r.

[14] H. Luo, L. Y. Liang, Q. Liu, and H. T. Cao, "Magnetron-sputtered SnO thin films for p-type and ambipolar TFT applications," *ECS J. Solid State Sci. Technol.*, vol. 3, no. 9, pp. Q3091–Q3094, Sep. 2014, doi: 10.1149/2.017409jss.

[15] Y. Li et al., "Extremely sensitive dependence of SnO_x film properties on sputtering power," *Sci. Rep.*, vol. 6, no. 1, pp. 1–9, Nov. 2016, doi: 10.1038/srep36183.

[16] S. J. Han, S. Kim, J. Ahn, J. K. Jeong, H. Yang, and H. J. Kim, "Composition-dependent structural and electrical properties of p-type SnO_x thin films prepared by reactive DC magnetron sputtering: Effects of oxygen pressure and heat treatment," *RSC Adv.*, vol. 6, no. 75, pp. 71757–71766, 2016, doi: 10.1039/c6ra08726d.

[17] T. Yang et al., "Preparation and characterization of p-type transparent conducting SnO thin films," *Mater. Lett.*, vol. 139, pp. 39–41, Jan. 2015, doi: 10.1016/j.matlet.2014.10.040.

[18] A. W. Lee, D. Le, K. Matsuzaki, and K. Nomura, "Hydrogen-defect termination in SnO for p-channel TFTs," *ACS Appl. Electron. Mater.*, vol. 2, no. 4, pp. 1162–1168, Apr. 2020, doi: 10.1021/acsaelm.0c00149.

[19] J. S. Jung, S. J. Park, J. H. Ye, J. G. Woo, B. S. Bae, and E.-J. Yun, "Optical, structural, and electrical properties of sputter-deposited SnO_x thin films," *Thin Solid Films*, vol. 747, Apr. 2022, Art. no. 139139, doi: 10.1016/j.tsf.2022.139139.

[20] M. J. Powell, C. van Berkel, A. R. Franklin, S. C. Deane, and W. I. Milne, "Defect pool in amorphous-silicon thin-film transistors," *Phys. Rev. B, Condens. Matter*, vol. 45, no. 8, pp. 4160–4170, Feb. 1992, doi: 10.1103/physrevb.45.4160.

[21] F. R. Libsch and J. Kanicki, "Bias-stress-induced stretched-exponential time dependence of charge injection and trapping in amorphous thin-film transistors," *Appl. Phys. Lett.*, vol. 62, no. 11, pp. 1286–1288, Mar. 1993, doi: 10.1063/1.108709.

[22] I.-C. Chiu and I.-C. Cheng, "Gate-bias stress stability of p-type SnO thin-film transistors fabricated by RF-sputtering," *IEEE Electron Device Lett.*, vol. 35, no. 1, pp. 90–92, Jan. 2014, doi: 10.1109/LED.2013.2291896.

[23] J. K. Jeong, H. Won Yang, J. H. Jeong, Y.-G. Mo, and H. D. Kim, "Origin of threshold voltage instability in indium-gallium-zinc oxide thin film transistors," *Appl. Phys. Lett.*, vol. 93, no. 12, Sep. 2008, Art. no. 123508, doi: 10.1063/1.2990657.

[24] L. K. J. Vandamme, X. Li, and D. Rigaud, "1/f noise in MOS devices, mobility or number fluctuations?" *IEEE Trans. Electron Devices*, vol. 41, no. 11, pp. 1936–1945, Nov. 1994, doi: 10.1109/16.333809.

[25] R. Hong et al., "Al_2O_3/HfO_2 bilayer dielectric for ambipolar SnO thin-film transistors with superior operational stability," *IEEE Trans. Electron Devices*, vol. 69, no. 8, pp. 4293–4297, Aug. 2022, doi: 10.1109/TED.2022.3184908.

[26] D. Rigaud, M. Valenza, and J. Rhayem, "Low frequency noise in thin film transistors," *IEE Proc.-Circuits, Devices Syst.*, vol. 149, no. 1, pp. 75–82, Feb. 2002, doi: 10.1049/ip-cds:20020063.

[27] J. Szubera et al., "XPS study of the L-CVD deposited SnO_2 thin films exposed to oxygen and hydrogen," *Thin Solid Films*, vol. 391, no. 2, pp. 198–203, Jul. 2001, doi: 10.1016/S0040-6090(01)00982-8.

[28] K.-H. Bae, M. G. Shin, S.-H. Hwang, H.-S. Jeong, D.-H. Kim, and H.-I. Kwon, "Electrical performance and stability improvement of p-channel SnO thin-film transistors using atomic-layer-deposited Al_2O_3 capping layer," *IEEE Access*, vol. 8, pp. 222410–222416, 2020, doi: 10.1109/ACCESS.2020.3043780.

[29] B.-E. Park, J. Park, S. Lee, S. Lee, W.-H. Kim, and H. Kim, "Phase-controlled synthesis of SnOx thin films by atomic layer deposition and post-treatment," *Appl. Surf. Sci.*, vol. 480, pp. 472–477, Jun. 2019, doi: 10.1016/j.apsusc.2019.03.013.

[30] W. Zhang et al., "Enhanced performance of p-type SnO_x thin film transistors through defect compensation," *J. Phys., Condens. Matter*, vol. 34, no. 40, Aug. 2022, Art. no. 404003, doi: 10.1088/1361-648X/ac8464.

[31] K. Mashooq, J. Jo, and R. L. Peterson, "Extraction of SnO subbandgap defect density by numerical modeling of p-type TFTs," *IEEE Trans. Electron Devices*, vol. 69, no. 5, pp. 2436–2442, May 2022, doi: 10.1109/TED.2022.3162803.

[32] K. Rajshekar et al., "Effect of plasma fluorination in p-type SnO TFTs: Experiments, modeling, and simulation," *IEEE Trans. Electron Devices*, vol. 66, no. 3, pp. 1314–1321, Mar. 2019, doi: 10.1109/TED.2019.2895042.

[33] J. B. Varley, A. Schleife, A. Janotti, and C. G. Van de Walle, "Ambipolar doping in SnO," *Appl. Phys. Lett.*, vol. 103, no. 8, Aug. 2013, Art. no. 082118, doi: 10.1063/1.4819068.

[34] H. Luo, L. Liang, H. Cao, M. Dai, Y. Lu, and M. Wang, "Control of ambipolar transport in SnO thin-film transistors by back-channel surface passivation for high performance complementary-like inverters," *ACS Appl. Mater. Interfaces*, vol. 7, no. 31, pp. 17023–17031, Aug. 2015, doi: 10.1021/acsami.5b02964.

[35] M. Minohara et al., "Elaboration of near-valence band defect states leading deterioration of ambipolar operation in SnO thin-film transistors," *Nano Select*, vol. 3, no. 6, pp. 1012–1020, Jun. 2022, doi: 10.1002/nano.202100272.

[36] T. Kim et al., "Origin of ambipolar behavior in p-type tin monoxide semiconductors: Impact of oxygen vacancy defects," *IEEE Trans. Electron Devices*, vol. 68, no. 9, pp. 4467–4472, Sep. 2021, doi: 10.1109/TED.2021.3099081.

[37] A. Togo, F. Oba, I. Tanaka, and K. Tatsumi, "First-principles calculations of native defects in tin monoxide," *Phys. Rev. B, Condens. Matter*, vol. 74, no. 19, Nov. 2006, doi: 10.1103/PhysRevB.74.195128.